RESEARCH PAPER

CrossMark

Virus concentration and purification by a microfluidic filtering system with an integrated PEGylated antifouling membrane

Sangil Kim[1,2,3] · Dietrich Dehlinger[1] · José Peña[1] · Hyang Seol[2] · Maxim Shusteff[1] · Nicole M. Collette[1] · Maher Elsheikh[1] · Matthew Davenport[1] · Pejman Naraghi-Arani[1] · Elizabeth Wheeler[1]

Abstract

We present the integration of a nanoporous membrane functionalized with hydrophilic polymer brushes, poly(ethylene glycol) methacrylate (PEGMA), into a microfluidic device. In order to prevent damage to functional groups on the membrane surfaces, the PEGMA-modified membrane was directly bonded using an intermediate UV-curable adhesive layer by employing the modified "Stamp-and-Stick (SAS)" method and operated at high pressures. We demonstrated that the degree of flux recovery (R_{FR}) of the functionalized membrane during testing with bovine serum albumin, that reached 93% after a cleaning process while unmodified membranes showed only 63% of R_{FR}. The viral particle recovery efficiency and concentration factor were 60.41% and 6.04, respectively.

1 Introduction

Numerous molecular techniques including quantitative polymerase chain reaction (qPCR) and quantitative reverse transcription-PCR (qRT-PCR) have been developed and applied to virus quantification from clinical samples. One big challenge facing some molecular detection applications (such as detection of bacteria in blood or salmonella in food) is the requirement for pre-concentration from large volumes (tens of milliliter) prior to sample preparation and qPCR/ qRT-PCR. Conventional concentration techniques are based on centrifugation, or direct membrane filtration (Hill et al. 2007; Karim et al. 2009; Liu et al. 2012; Mull and Hill 2009; Rajal et al. 2007; Rutjes et al. 2005).

This type of sample concentration is readily addressed in a centrifuge-equipped conventional laboratory, however, such methods necessitate complex processing by skilled technicians using costly large-scale instrumentation (Zhang et al. 2013a). For example, an ultracentrifuge is often required for concentration of viral samples. Due to the cumbersome and slow centrifugation processes, modern virus concentration techniques typically utilize far faster, safer and simpler direct filtration techniques. Typically, negatively charged cellulose membrane filters are used to adsorb and concentrate positively charged viruses when the pH of the solution is below the isoelectric point of the viruses. However, direct filtration may not efficiently retain the nano-sized virus particles on the membrane resulting in greater than 2-log losses of viral particles that can cause significant negative effects on virus concentration and detection (Zhang et al. 2013b).

Microfluidic diagnostic platforms provide significant advantages over conventional lab-scale instruments, including improvements in sample-to-answer times, lower reagent consumption, portability, and ease of integration and automation of multiple analytical processing steps (Park et al. 2011). The integration of porous membranes into microfluidics has attracted substantial attention over the last decade (Amato et al. 2012; Ji et al. 2008; Wang et al. 2012; Zheng et al. 2007). Compared to other microfluidic chip-based approaches such as electrophoretic/dielectrophoretic flow (Chen and Du 2007; Dürr et al. 2003; Puchberger-Enengl et al. 2011), optical tweezing (Lin et al. 2008), shear-induced

✉ Sangil Kim
  sikim@uic.edu

1 Lawrence Livermore National Laboratory, Livermore, CA 94550, USA

2 Department of Chemical Engineering, University of Illinois, Chicago, IL 60607, USA

3 Department of Chemical & Petroleum Engineering, University of Pittsburgh, Pittsburgh, PA 15261, USA

forces (Di Carlo et al. 2007, 2008), magnetic forces (Kang and Park 2007; McCloskey et al. 2003), and evaporation (Ho et al. 2012; Zhang et al. 2013a), a microfluidic device integrated with a membrane filter is simple, inexpensive, and does not require extra steps such as labeling (Amato et al. 2012; Ji et al. 2008; Wang et al. 2012; Zheng et al. 2007). However, the membrane-based microfluidic devices require further improvements on membrane fouling and clogging. Hence, the ideal membrane for this application needs to incorporate antifouling functionality to effectively separate viral particles from cell waste. Without antifouling coatings, viruses and cell debris rapidly clog the membrane pores or surfaces thereby interfering with the separation process and resulting in vast reductions in process speed and viral purity. In addition, many of the technologies reported so far have suffered from fluid leakage around membranes due to prolonged exposure to the high pressures caused by membrane fouling.

Various approaches to bonding membranes to microfluidic devices have been reported such as direct bonding (Aran et al. 2010) and bonding with an intermediate layer (Satyanarayana et al. 2005). Direct thermal bonding can create permanently laminated structures, but also tends to cause wrinkling of the membrane, or distortion and collapse of the membrane pores (Aran et al. 2010). Oxygen plasma activation of the polydimethylsiloxane (PDMS) and membrane surface followed by direct bonding also can create laminated structures. However, this method can only create weak Si–O–C bonds which are hydrolytically unstable and often fail in aqueous environments (Lee and Ram 2009). Moreover, the direct bonding methods are not suitable for integration of functionalized membranes into microfluidic devices because heat or oxygen plasma can degrade the chemical functional groups on the membrane surface. Direct bonding methods use epoxy or PDMS prepolymer as an intermediate bonding layer between the PDMS and the membrane and these methods can significantly improve the bonding strength (Wu and Steckl 2009). However, this approach can cause partial clogging of the membrane pores and thus reduce the flux across the membranes. In addition, bonding with a thermal-curing material requires high-temperatures that can affect functional groups on the membrane. Approaches using UV-curable materials have recently gained popularity because UV-curing is much faster than thermal-curing and more importantly, the curing process is performed at room temperature. "Stamp-and-Stick (SAS)" techniques using UV-curable adhesives can provide strong bonding and the microfluidic devices fabricated from this method can operate at high pressures. However, there is a need for enhanced control on the application of the gluing layer on to the functionalized membranes.

The purpose of the work here is to design and fabricate a viral filtering microfluidic device which can autonomously and continuously concentrate viral particles. The three main objectives of this work were: (1) separate viral particles from cell waste (purification); (2) concentrate viral particles (concentration), and (3) efficiently recover concentrated viral particles (recovery). In order to achieve this, we have developed a viral filtration device with high viral retention and recovery by incorporating a poly(ethylene glycol) methacrylate (PEGMA) functionalized membrane into the microfluidic device. In this study, we used dengue virus as a model of viral particles filtration. The PEGMA-functionalized nanoporous membrane provided high viral separation efficiency arising from hydration of functional polymer layers and their resistance to protein adsorption. In order to prevent degradation of the PEGMA functional groups from direct thermal curing or oxygen plasma bonding method, and pore clogging caused by direct UV-curable glue coating on the surface of PDMS microchannels, we precisely controlled the thickness of the glue layer by employing the modified SAS method (Satyanarayana et al. 2005), so the functionalized membrane is directly bonded using an intermediate UV-curable adhesive layer to prevent partial clogging of membrane and to operate the device at high pressures without leakage over extended periods of operation.

2 Materials and methods

2.1 PDMS microchannel fabrication

Silicone elastomer microfluidic devices were fabricated by multilayer soft lithography, as a modification of the general approach first described by Thorsen et al. (2002). Figure 1 shows a schematic of the microchannel device design, main flow channel, membrane filtration region, and a photo of the assembled device. Briefly, a mold for casting the sample flow channels (FC, blue features in Fig. 1a–d) was produced by spinning a 10-µm layer of positive photoresist (AZ50XT) on a 100-mm silicon wafer. After softbaking, exposure and development, a "reflow" hot plate bake at 135 °C for 30 s produced rounded profiles to allow full closure of fluidic valves. The second mold for casting control channels and valves (CC, red features in Fig. 1a, d) was fabricated by spinning a 30-µm-thick layer of SU-8 2025 (MicroChem, Newton, MA, USA) on a silicon wafer. The SU-8 was processed according to the manufacturer's recommended process parameters to generate features with rectangular profiles. All control line widths were designed to be 25 µm, except in locations where valve functionality is desired, where they were 150 µm wide. The third mold, for the filtration channels (FILT, green features in Fig. 1a, c, d) was made from 20-µm-thick SU-8 25. Prior to casting of PDMS layers, all masters were treated with
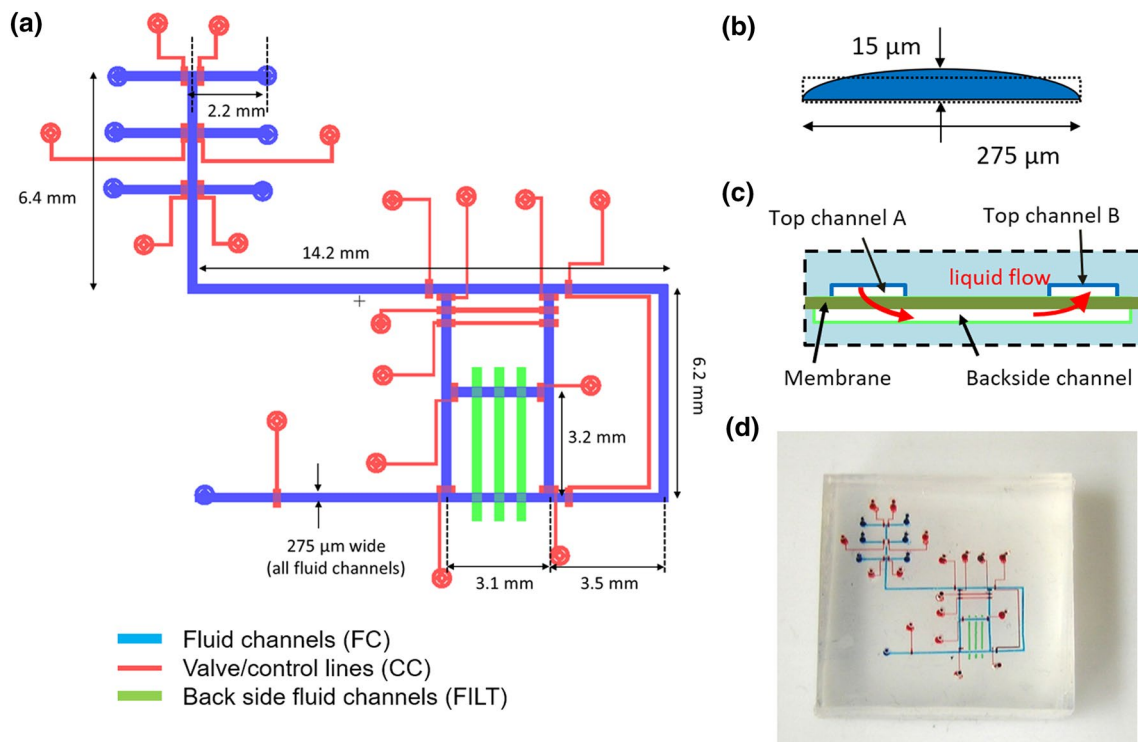
Fig. 1 Microfluidic chip designs. **a** Schematic of device. The FC is top channel and the FLIT is back side channel. **b** Fluid channel profile. Due to re-flowed photoresist, it initially spun 10 µm thick. Assume cross-sectional area equivalent to 10-µm-high channel, volume of the chamber is approximately 2.75 nL per mm length. **c** Membrane filtration channel profile. After viral particles are filtered out in the top channel A (FC) and liquid transports through membranes to the backside channel (FLIT). The filtered liquid transports back to the top channel B (FC) through the membrane afterward. **d** A picture of the assembled microfluidic device

trichloromethylsilane to aid as a mold release by evaporating under vacuum for 5 min.

The device layers were cast at different mix ratios of the PDMS components (RTV615, Momentive Performance Materials, Columbus, OH, USA). The top (thick, CC) control layer was mixed at a 5:1 ratio of parts *A:B*, producing a stiffer silicone than the standard 10:1 recipe. After pouring onto the CC mold to a depth of 6–8 mm, and de-gassing for 15 min under vacuum, the layer was partially cured in a convection oven at 80 °C for 30 min. The middle (thin, FC) layer was mixed at a 20:1 ratio of *A:B*, a more compliant material. This mixture was spun onto the reflowed FC mold at 2000 RPM for 1 min, and allowed to relax for 5 min in ambient air, allowing the layer to self-planarize to a thickness of approximately 25 µm. This layer was similarly part-cured at 80 °C for 15 min. Individual devices were cut out of the CC layer, control access ports were cut with a round 0.65 mm ID, 900 µm OD punch (Syneo, Angleton, TX, USA) then each device was aligned and contacted to its corresponding thin (FC) layer still on its mold wafer. The two layers were then fully cured at 80 °C for 8 h to achieve full bonding strength, and peeled from the FC mold to prepare for membrane attachment.

The bottom (FILT) device slab was cast at the standard 10:1 mix ratio of parts *A:B*, poured 6–8 mm thick, vacuum degassed, as above, fully cured for 8 h at 80 °C, and peeled from its mold in preparation for membrane bonding.

2.2 Surface-initiated PEGMA copolymerization

For surface modification of the membranes, surface-initiated atom transfer radical polymerization (ATRP) was employed as described elsewhere (Chang et al. 2009). Briefly, plasma-activated, track-etched polyester (Sterlitech, WA, USA) membranes were placed in 50 mL deionized water (DI) at 80 °C for 2 h. After drying at RT under vacuum, the treated membranes were immersed into 30 mL of 2-bromoisobutyryl bromide (BIBB, 98%) in hexane. After slow addition of 0.5 g triethylamine at 4 °C for 15 min, the system was allowed to react at room temperature for 1 day. After the reaction, the Br-functionalized polyester membrane (PET-Br) was transferred into purified hexane and washed with ethanol and DI water several times. The prepared PET-Br membranes were placed in 30 mL of 5 wt% PEGMA macromonomer solution in methanol for 12 h and a purified argon stream was introduced to de-gas the solution in a single-necked round-bottom flask for about 10 min. Cu(I)

Br (22.7 mg) and 2,2-bipyridine (50.0 mg) were sequentially added to the solution, and the reactor flask with solution was purged with purified nitrogen at 25 °C under constant stirring. After the reaction, the PEGMA-grafted PET membranes were transferred into purified methanol and washed with DI water several times.

2.3 Membrane bonding onto a PDMS device

In order to bond the membranes onto PDMS microfluidic channels, the Stamp-and-Stick method was employed (Satyanarayana et al. 2005). Figure 2 shows the overall process for bonding the functionalized membrane onto each PDMS layer. First, UV-curable adhesive (NEA 121, Norland Product) was spin-coated at 5000 rpm for 2 min to obtain a thin glue layer on a silicon wafer. Then, an air plasma surface-treated (5 min, 30 W, Harrick Plasma) PDMS slab with patterned channels (FC and CC layers) was brought into contact with the adhesive. Once the adhesive layer was transferred to the PDMS slab, the pristine or modified membrane was transferred onto the adhesive on the PDMS slab and the PDMS/membrane device was immediately exposed to UV radiation for 10 min to prevent wetting of UV-glue on the membrane surface in the channel. For the second bonding, same method as the first PDMS and membrane was used except special care was taken to align microchannels on two PDMS slabs. The final device was cured by exposure to UV radiation for 10 min. If necessary, the device was cured further using additional heat-curing at 60 °C overnight.

2.4 Characterization

Contact angle measurements were performed using a Krüss drop shape analysis (DSA) 100. Briefly, the instrument is interfaced with a computer allowing the user to control liquid dosing, sample illumination and image capture. For these experiments, a 2-µL droplet of DI water is dispensed onto the surface of the membrane and allowed to rest for 2 min to reach an equilibrium shape before using the DSA software

to capture an image of the droplet and measure the contact angle. At least three such measurements were made for each sample.

For membrane filtration experiments, a dead-end cell filtration test was carried out to characterize the protein and virus filtration performance and water flux recovery ratio of the prepared membranes. Before the filtration tests, the pristine or PEGMA-grafted membranes were pre-wetted in DI water for 30 min. After the first pure water flow rate measurement, a protein fouling test was performed using a 1 mg/ml solution of bovine serum albumin (BSA) in 0.1 M phosphate buffered saline (PBS). Then, the protein filtration-tested membranes were washed with DI water under stirring for 1 h followed by a second pure water permeance measurement. For viral filtration tests, a solution of cultured dengue virus (3.5×10^4 virions/ml) was filtered through the membrane. Viral concentrations in permeate solution after membrane were determined using qRT-PCR. Measurements were performed several times (at least four) in order to check consistency of the data.

2.5 qRT-PCR viral genome quantification

The operation of the microfluidic device was as follows. A solution containing dengue virus was loaded in the sample storage vial and a wash buffer solution was separately loaded in another storage vial. The viral particle solution was then pumped through the device at 5 psi, where filtration and concentration of the viral particles occurred as the dengue viruses were filtered out by the functionalized membrane incorporated in the device. Filtered and concentrated viral particle solutions were collected from the exit port for qRT-PCR analysis. For the prepared devices, the test was repeated several times (at least four) and average values with standard deviation were recorded.

All reactions were performed on 96-well FAST PCR plates (Applied Biosystems, Foster City, CA) in a total volume of 25 µl (20 µl master mix plus 5 µl sample) optimized for quantitative reverse transcriptase polymerase chain reaction
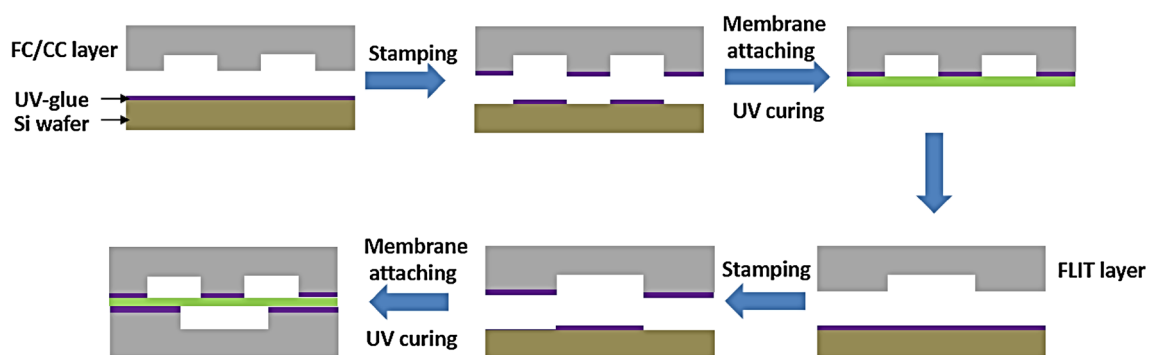

Fig. 2 A schematics of the PEGMA-*g*-PET membrane bonding

(qRT-PCR). A volume of 20 μl qRT-PCR master mix was prepared per manufacturer instructions (AgPath-ID™ One-Step RT-PCR Kit, Life Technologies, Foster City, CA). Reactions were performed on ABI 7500 thermal cyclers (Life Technologies) under the following real-time fast thermal cycling conditions: 45 °C for 10 min for reverse transcription of cDNA synthesis, 95 °C for 10 min for inactivation of the reverse transcriptase, activation of 25× RT-PCR Enzyme Mix, and denaturation of the RNA/cDNA hybrid; followed by amplification at 40 cycles of 97 °C for 2 s and 60 °C for 30 s. Oligonucleotide primers and probes were purchased from Biosearch Technologies, Inc. (Novato, CA). Primer and probe sequences were as follows: forward primer 5′CATATTGACGCTGGG AAAGAC3′ and reverse primer 5′TTCCATTTTCTGGCG TTCTGTG3′. Upon receipt, oligos were reconstituted in sterile 1× Tris-EDTA buffer (10 mM Tris-Cl, 1 mM EDTA, pH 8.0, Teknova, Hollister, CA) to a concentration of 100 mM. Working stocks were made by diluting primers and probes to a concentration of 10 mM with Tris-EDTA buffer.

A standard curve of C_t vs. amount of infectious virus RNA was generated and used to determine the plaque forming units (PFU) equivalent viral RNA amounts reported using standard plaque assays on baby hamster kidney (BHK) cells and total RNA from viral culture supernatants.

3 Results and discussion

3.1 Contact angle measurement for unmodified and functionalized membranes

The hydrophilicity of the PEGMA-*g*-PET membranes was evaluated by measuring water contact angle of the membranes. The pristine PET membrane showed a water contact angle of 83.35°, corresponding to high hydrophobicity of the membrane surface, while the PEGMA-*g*-PET membrane had a lower contact angle value of 72.55°. The decrease in water contact angle of the membrane after functionalization indicated that the introduction of PEGMA on the membrane surface could increase surface coverage on the hydrophobic membranes, thus enhancing the hydrophilicity of the PET membranes. This result is consistent with the performance of other hydrophilic functional group-grafted membranes (Chang et al. 2009; Su et al. 2008).

3.2 Flow rate recovery filtration test using BSA and dengue virus

The water flow rate was recorded periodically and water permeance (J_w) was calculated by the following equation:

$$J = \frac{V}{A \Delta t}, \tag{1}$$

where J, V, A, and Δt denote the water permeance, water permeate volume, membrane area, and time. The rejection ratio of dengue virus (R_{dengue}) was calculated by the following equation:

$$R_{dengue} = \left(1 - \frac{C_p}{C_f}\right) \times 100\%, \tag{2}$$

where C_p and C_f (virions/ml) are dengue virus concentrations of permeate and feed sides, respectively. All experiments were operated at 2 psi without stirring to simulate the membrane filtration conditions expected inside microchannel devices.

To investigate the antifouling property of the functionalized membrane, the degree of flux recovery (R_{FR}), the degree of total flux loss (R_t), the degree of flux loss due to reversible protein fouling (R_r), and the degree of flux loss caused by irreversible fouling (R_{ir}) that cannot be eliminated using hydraulic cleaning process were calculated. The ratios were calculated by the following equations:

$$R_{FR} = \frac{J_{w2}}{J_{w1}}, \tag{3}$$

$$R_t = 1 - \frac{J_{BSA}}{J_{w1}}, \tag{4}$$

$$R_r = \frac{J_{w2} - J_{BSA}}{J_{w1}}, \tag{5}$$

$$R_{ir} = \frac{J_{w1} - J_{w2}}{J_{w1}}, \tag{6}$$

where subscript w1, w2, and BSA denote the water permeance before BSA test, after BSA test, and during BSA test, respectively. Figure 3 shows the time-dependent flux of the virgin PET membrane and the PEGMA-*g*-PET membrane and a summary of R_{FR}, R_t, R_r, and R_{ir} of the pristine and PEGMA-modified PET membranes are shown in Table 1. Water fluxes (J_{w1} and J_{w2}) of the PEGMA-*g*-PET membrane are higher than that of the pristine PET membrane which agree well with the results of the increased hydrophilicity by the grafting discussed in the contact angle measurement. This is because the hydrophilicity of the PEGMA-*g*-PEM membrane can influence the water flux more effectively than the pore size decrease by the functionalization (Chang et al. 2008). The permeation flux of BSA solution on the membrane before PEGMA grafting decreased rapidly to 80% of pure water flux due to protein fouling on the membrane surface. After cleaning the unmodified membrane with DI water, R_{FR} of the membrane is only 63%. However, R_{FR} of the PEGMA-*g*-PET membrane reached 93% of R_{FR} after cleaning indicating lower persistence BSA adsorption

(a)

(b)
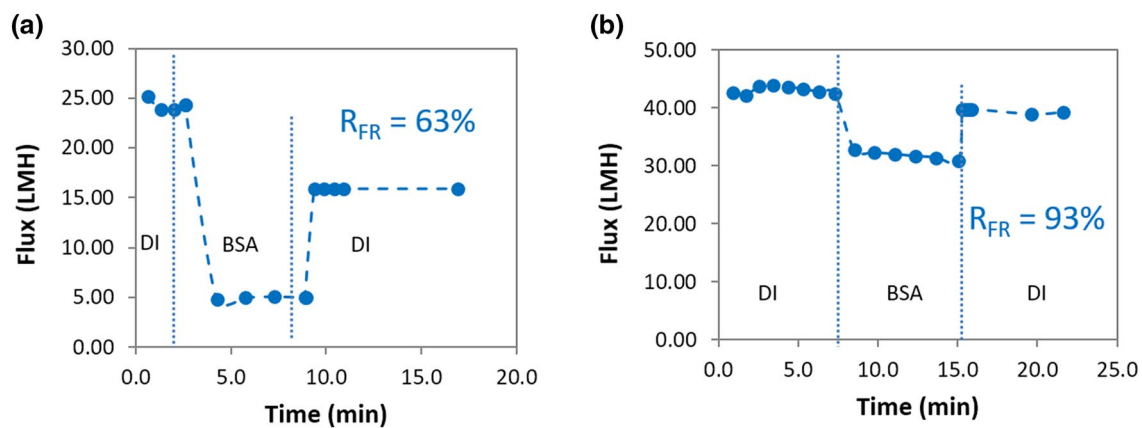
Fig. 3 BSA filtration performance of PET membrane: **a** before PEGMA grafting, and **b** after PEGMA grafting

onto the functionalized membrane surface. This result is

Table 1 A summary of BSA antifouling properties of PET membranes (100 nm pore size)

Membrane	R_{FR} (%)	R_t	R_r	R_{ir}
PET	64.69 ± 3.86	0.79 ± 0.01	0.44 ± 0.03	0.35 ± 0.03
PEGMA-g-PET	92.62 ± 0.44	0.27 ± 0.00	0.19 ± 0.01	0.08 ± 0.00

consistent with antifouling performance ($R_{FR} = 91\%$) of PEGMA-grafted PVDF membranes for ultrafiltration tests conducted by others (Chang et al. 2009). Moreover, the PEGMA-grafted PET membrane shows lower total flux loss ($R_t = 0.28$) compared to the unmodified PET membrane ($R_t = 0.80$). The lower R_t indicates lower total flux loss because of less BSA adsorption or deposition on the membrane surface. Table 1 also shows that the R_{ir} decreased remarkably from 0.35 to 0.08 after introduction of PEGMA on the PET membrane surface. The R_r value contributed by the loosely attached proteins decreased from 0.45 to 0.2 with the PEGMA modification. It has been reported that the introduction of PEGMA on hydrophobic membrane surfaces could significantly reduce membrane fouling because BSA was less adherent to the more hydrophilic membrane surface and could thus be more easily washed off (Chang et al. 2009; Su et al. 2008). In particular, membrane modification with PEGMA substantially reduced irreversible membrane fouling. The highly hydrophilic polymer brushes may be responsible for this reduction in membrane fouling. These polymer brushes hold a large relative amount of free water on the membrane surfaces and this water layer can be associated with surfaces containing hydrophilic functional groups preserved the native properties of the adsorbed proteins (Su et al. 2008). As a result, the PEGMA-g-PET membranes show higher water flux recovery compared to the pristine

PET membrane. We also compared the antifouling performance of the PEGMA-g-PET membrane with oxygen plasma-treated PET membrane (o-PET). Initial water flux of the o-PET membrane was slightly higher than pristine PET membrane due to improved hydrophilicity. However, the R_{FR} value of o-PET membrane was similar to that of the pristine PET membrane indicating that antifouling effect of oxygen plasma method is not effective.

3.3 SEM images of membranes before/after BSA filtration

Figure 4 shows SEM images of PEGMA-g-PET membrane and pristine membrane surfaces before and after filtration and washing tests (Fig. 4a–d). The SEM images of PEGMA-g-PET membrane (Fig. 4e, f) clearly show that BSA cake formation was remarkably suppressed on the functionalized membrane surface and almost no cake was observed to be adhered to the functionalized membrane surface as compared to the pristine PET membrane surface after the BSA filtration test (Fig. 4c, d). In addition, the functionalized membrane maintained close to the same pore size as the pristine membrane before the filtration test while the unmodified membrane suffered pore size decreases in the 20–60 nm after BSA filtration and washing. These SEM results correspond to the result of the flow rate recovery filtration test using BSA and strongly suggest that the hydrophilic surface of PEGMA-g-PET membranes could efficiently suppress BSA adhesion on the membrane surface and enhance the antifouling properties of the membrane.

3.4 Dengue virus filtering test and PCR analysis

Viral filtration efficiencies of the functionalized membranes with different pore sizes were investigated using dengue virus (particle diameter 40 nm). Viral concentrations in
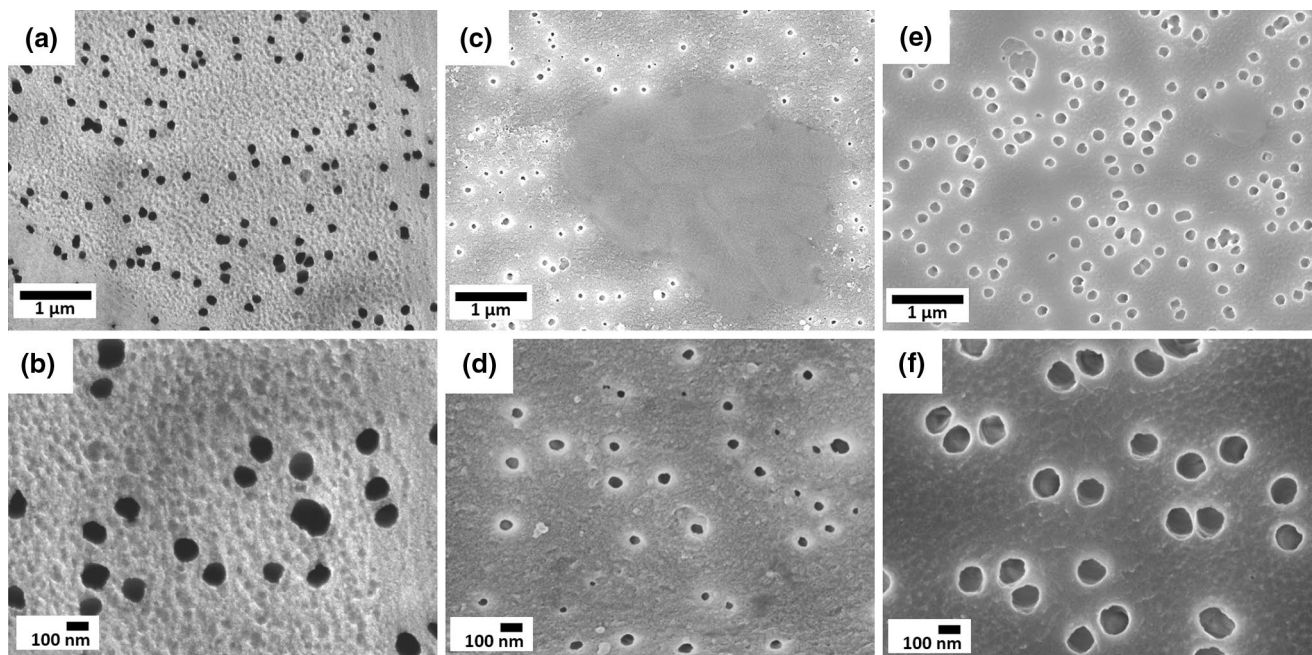
Fig. 4 SEM images of membrane surface. **a** and **d** are surface of pristine PET membrane before BSA test, **b** and **e** are surface of pristine PET membrane after BSA test, **c** and **f** are surface of PEGMA-*g*-PET membrane after BSA test. **a–c** are low magnification of SEM images and **d–f** are high magnification of SEM images

Table 2 Viral filtering efficiency of the functionalized membranes with different pore diameters

	Viral filtering efficiency (PCR, %)	Water flux (LMH/bar)
100 nm PEGMA-*g*-PET	> 99	42.35 ± 0.87
50 nm PEGMA-*g*-PC	> 98	21.40 ± 0.75
30 nm PEGMA-*g*-PC	100	4.79 ± 0.08

feed and filtered solution were analyzed using qRT-PCR. Table 2 shows the viral filtering efficiency of 30, 50, and 100 nm pore PEGMA-grafted membranes. The membrane with 30-nm pores completely excluded the 40-nm viral particles as expected, but showed lower flux. Interestingly, membranes functionalized with 100- and 50-nm pores also could filter out dengue virus while maintaining high water flux. This is because the PEGMA brushes can form a continuous hydration layer on the membrane surface and provide this layer an adsorption resistance against the dengue virus particles and thus prevent the virus particles from entering the pores (Chang et al. 2009). Therefore, we chose a functionalized membrane pore size of 100 nm for device fabrication due to its ability to exclude dengue virus while maintaining higher water flux. In future work, we will further investigate the effect of particle size on the filtration performance to establish virus size and pore size relationship.

3.5 Pressure test of the device (adhesive bond strength/valve pressure test)

The use of the Stamp-and-Stick bonding method for PDMS microchannels and PEGMA-PET membrane bonding allowed the fabrication of complex microchannel designs with integrated functionalized membranes and multi-layer PDMS channels. The bonding strength of the PEGMA-modified PET membrane and PDMS assembly was measured via leak test by injecting a dye solution into the microchannel. Most tested devices at room temperature could withstand pressures of 30 psi without showing any visible leaks. Leak-free bonding of the functionalized membrane was demonstrated for 4 days at 15 psi using dye solutions at room temperature. As shown in Fig. 1d, the dye solution-injected device shows no visible leak in the channels. Furthermore, this demonstrates that UV-glue used to bind the functional membranes does not clog or distort the microchannels. This result shows that the bonding is leak-free along the microchannels, and the hydrolytic stability of the device enabled testing of the device using dengue virus in this study.

Microchannel structures were examined using SEM after the devices were sliced perpendicularly to the channel. Achieving a thin and strong adhesive bonding layer is crucial because the height of the channels in this study is ca. ~40 μm and the adhesive layer should maintain its thickness with respect to the height of the microchannel. The SEM image of the channel in Fig. 5 shows no thick adhesive
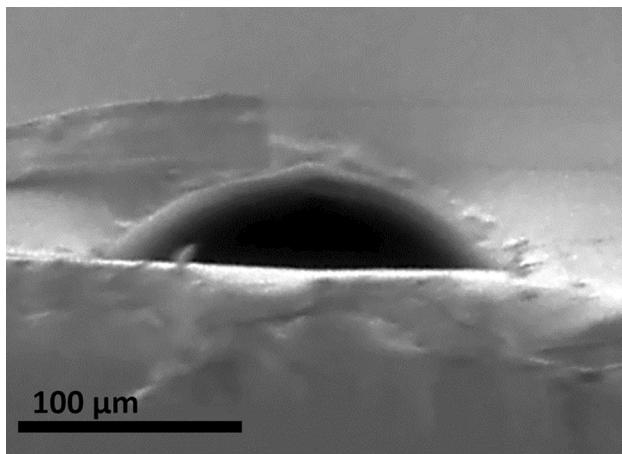
Fig. 5 SEM images of the microfluidic channel free of thick adhesive layer or clogging

layer and open channel. A photo of the assembled device filled with different colors of dyes provides evidence of free-flowing channels in the device.

3.6 Viral particle recovery

Figure 6 illustrates the viral particle recovery and concentration procedures. Filtered fluid is the fluid that passed through the PEGMA-*g*-PET membranes incorporated in the device (Fig. 6a). The 100 μl of dengue virus solution ($C_0 = 5.33 \times 10^4$ virions/ml) was introduced into the inlet with a pressure of 5 psi and 10 μl of the filtered fluid was collected for the qRT-PCR analysis. The chip wash fluid is the fluid that washes around the membrane filtering region after the region with the membrane is isolated from the rest of the chip by sealing off the valves (Fig. 6b). Membrane wash fluid is the fluid that passed over the membrane filter region of the chip after filtering (Fig. 6c). This process was achieved by opening the valves sealing the filter region from the exit port of the microfluidic device. All collected samples were amplified using qRT-PCR as described in the experimental section.

Figure 7 shows the viral recovery performance results of the prepared microfluidic device. PCR data show the filtered fluid has a high C_t value suggesting low viral concentration is in the solution. This is consistent with the result of high dengue virus filtration performance of PEGMA-*g*-PET membranes described in the previous section. In addition, this result suggests that our microfluidic device has leak-free valves because the PCR results should show high virus concentration in the filtered solution if the fluid moved through leaking valves instead of passing through the PEGMA-*g*-PET membranes. For the analysis of the membrane wash fluid, we ran several successive flushes of the filtration region. The PCR data show that the first wash solution

Fig. 6 Microfluidic chip operation mode. **a** Filtration mode. In this ▶ mode, fluid pass through the PEGMA-*g*-PET membrane and viral particles are collected on the membrane surface. **b** Chip wash mode. Water and buffer fluid wash around the membrane filtering region. **c** Membrane wash mode. Water and buffer fluid passes over the membrane filtering region of the chip after filtration mode

contained high concentration of virus and low concentration of virions were detected in subsequent washes. This result indicates that we achieved highly purified viral solution that is not adsorbed to the functionalized membrane, allowing for not only successful filtration, but adequate retrieval of the filtered sample for subsequent downstream analysis as well. Subsequent membrane wash solutions showed high C_t values and very low viral concentration, similar to the filter solution without viral particles. This result suggests that high amount of virus was recovered in the first wash and the viral particles floated on PEGMA-*g*-PET membrane surface without fouling, which is consistent with the result of the BSA flow rate recovery test and SEM studies of the membrane surfaces.

From the qRT-PCR data, the viral particle recovery efficiency and concentration factor were calculated as follows:

$$\text{Recovery (\%)}$$
$$= \frac{\text{Dengue viral load in the membrane wash solution}}{\text{Dengue viral load in the feed solution}} \times 100\%$$

(7)

$$\text{Concentration factor} = \text{Recovery (\%)} \times \frac{\text{Feed solution volume}}{\text{Output solution volume}}.$$

(8)

We injected 100 μl with 5.33×10^4 virions/ml and recovered 10 μl with $(3.22 \pm 0.13) \times 10^5$ virions/ml for the qRT-PCR analysis. The total processing time was 30 h which is slightly longer than the expected 26 h from the membrane surface area of 2.27×10^{-7} m^2 of and 42 L/(m^2 h bar) of membrane permeance. The calculated average dengue virus recovery ratio was $60.41 \pm 2.44\%$ with a corresponding concentration factor of 6.04 ± 0.24. The recovery ratio of our device is comparable to other membrane-incorporated microfluidic virus concentration devices ranging from 60% up to 82% (Wang et al. 2012; Zhang et al. 2013a). It should be noted that our device has advantages over the simple filter-based or membrane-based evaporation devices such as room temperature operation and no membrane clogging issue for longer test time. In addition, the channel volume at membrane wash mode was only 120 nl and the concentration factor achieved could be higher if the volume ratio between the feed (100 μl) and output volume (10 μl) was further increased (higher than 10).

We observed some viral particles were recovered as well during chip wash. This is because PDMS is prone to adsorbing proteins and hydrophobic molecules, and the
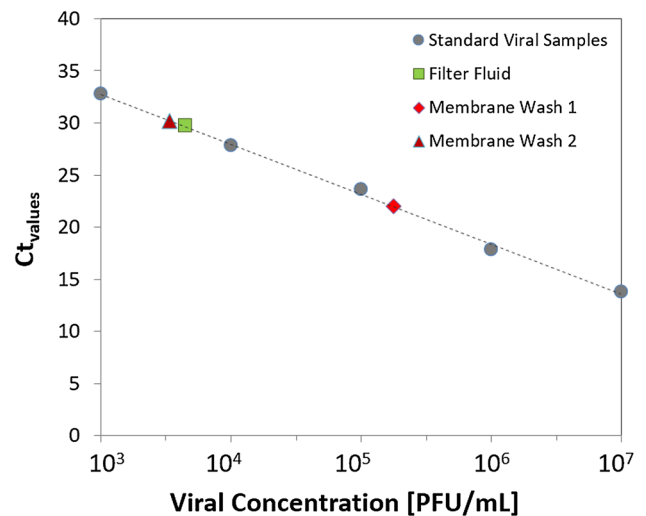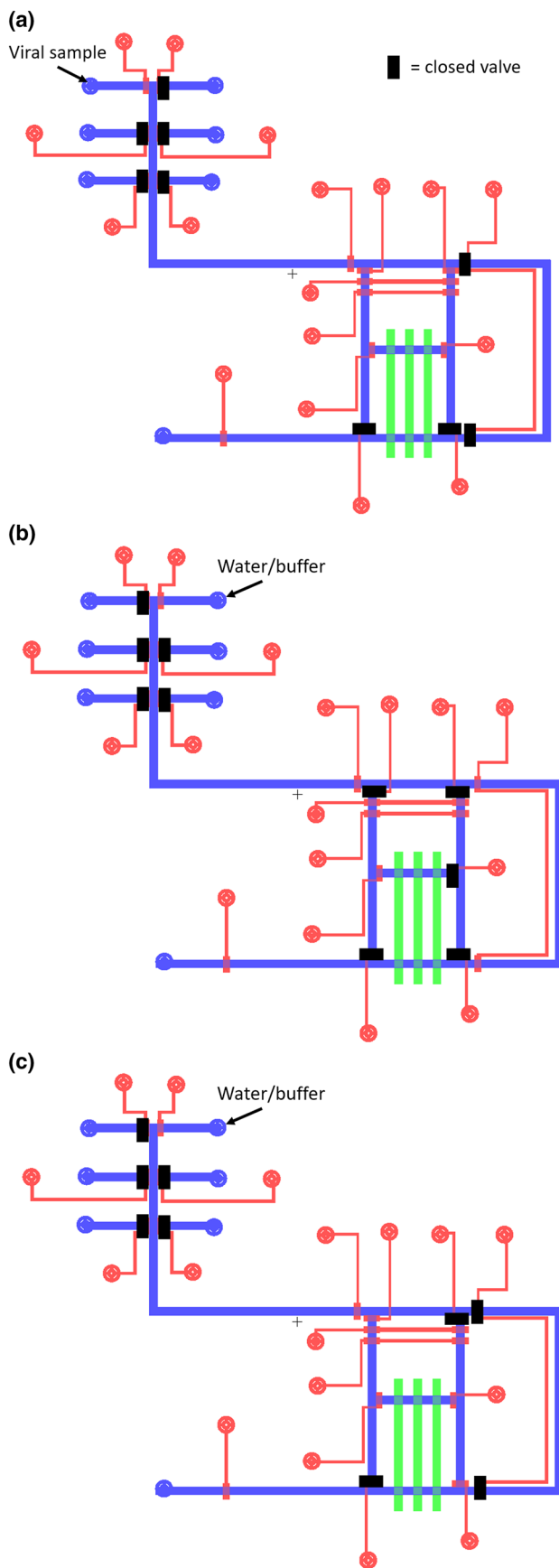
(a)

Viral sample

= closed valve

(b)

Water/buffer

(c)

Water/buffer

Fig. 7 Comparison of C_t value for the filter fluid and membrane wash solutions

microchannels were not functionalized with PEGMA groups to protect against protein adsorption on their walls (Boxshall et al. 2006). In future work, we will selectively functionalize the microchannels surface of the device with the antifouling polymer brushes (e.g., PEGMA) to prevent adsorption of viral particles on the channel surface and thus, to increase recovery ratio. We will also quantitatively analyze viral particles on the membrane surface to determine the amount of absorbed viral particles both on the membrane surface and PDMS channels.

4 Conclusions

By incorporating a PEGMA-grafted track-etched (PEGMA-g-PET) nanoporous membrane into the microfluidic device using the SAS technique, we have succeeded in fabricating a durable, disposable, and highly effective viral filtering microfluidic device, which can continuously concentrate viral particles. The degree of flux recovery (R_{FR}) of the PEGMA-g-PET membrane after BSA treatment reached 93% after cleaning process while unmodified membranes showed only 63% of R_{FR}, suggesting that the PEG-functionalized nanoporous membrane could provide high viral separation efficiency due to strong hydration of functional polymers layer and their resistance to protein adsorption. The functionalized membrane was directly bonded using an intermediate UV-curable adhesive layer employing the modified SAS method and operated at high pressures with no evidence of the PEGMA-functionalized membrane leakage or membrane pore clogging over an extended period of operation. When we tested our functionalized membranes with dengue virus particles, PCR results showed that the

filtered fluid had a low viral concentration and our microfluidic device has leak-free valves. The calculated viral particles recovery efficiency and concentration factor were 60% and 6, respectively, confirming our hypothesis based on our BSA testing results. The system in this study could apply to multiple surface functionalizations in different locations on a chip as well as efficient viral separation function to achieve high viral concentration, which would allow this methodology to be enabled for the development of exquisitely sensitive diagnostic tests in a clinical setting. For example, the chip could have adhesion area for the cells to form into confluent layers and remain adherent over the experiment, but at the same time, could contain antifouling functionality to separate viral particles from cell waste.

References

Amato L, Gu Y, Bellini N, Eaton SM, Cerullo G, Osellame R (2012) Integrated three-dimensional filter separates nanoscale from microscale elements in a microfluidic chip. Lab Chip 12:1135–1142. https://doi.org/10.1039/C2LC21116E

Aran K, Sasso LA, Kamdar N, Zahn JD (2010) Irreversible, direct bonding of nanoporous polymer membranes to PDMS or glass microdevices. Lab Chip 10:548–552. https://doi.org/10.1039/b924816a

Boxshall K, Wu M-H, Cui Z, Cui Z, Watts JF, Baker MA (2006) Simple surface treatments to modify protein adsorption and cell attachment properties within a poly(dimethylsiloxane) micro-bioreactor. Surf Interface Anal 38:198–201. https://doi.org/10.1002/sia.2274

Chang Y, Shih Y-J, Ruaan R-C, Higuchi A, Chen W-Y, Lai J-Y (2008) Preparation of poly(vinylidene fluoride) microfiltration membrane with uniform surface-copolymerized poly(ethylene glycol) methacrylate and improvement of blood compatibility. J Memb Sci 309:165–174

Chang Y et al (2009) Surface grafting control of PEGylated poly(vinylidene fluoride) antifouling membrane via surface-initiated radical graft copolymerization. J Memb Sci 345:160–169. https://doi.org/10.1016/j.memsci.2009.08.039

Chen D, Du H (2007) A dielectrophoretic barrier-based microsystem for separation of microparticles. Microfluid Nanofluid 3:603–610. https://doi.org/10.1007/s10404-007-0151-x

Di Carlo D, Irimia D, Tompkins RG, Toner M (2007) Continuous inertial focusing, ordering, and separation of particles in microchannels. Proc Natl Acad Sci USA 104:18892–18897. https://doi.org/10.1073/pnas.0704958104

Di Carlo D, Edd JF, Irimia D, Tompkins RG, Toner M (2008) Equilibrium separation and filtration of particles using differential inertial. Focus Anal Chem 80:2204–2211. https://doi.org/10.1021/ac702283m

Dürr M, Kentsch J, Müller T, Schnelle T, Stelzle M (2003) Microdevices for manipulation and accumulation of micro- and nanoparticles by dielectrophoresis. Electrophoresis 24:722–731 https://doi.org/10.1002/elps.200390087

Hill VR, Kahler AM, Jothikumar N, Johnson TB, Hahn D, Cromeans TL (2007) Multistate evaluation of an ultrafiltration-based procedure for simultaneous recovery of enteric microbes in 100-liter tap water samples. Appl Environ Microbiol 73:4218–4225. https://doi.org/10.1128/aem.02713-06

Ho NT, Fan A, Klapperich CM, Cabodi M (2012) Sample concentration and purification for point-of-care diagnostics. In: 34th annual international conference of the IEEE EMBS, 28 August–1 September, pp 2396–2399. https://doi.org/10.1109/EMBC.2012.6346446

Ji H, Samper V, Chen Y, Heng C, Lim T, Yobas L (2008) Silicon-based microfilters for whole blood cell separation. Biomed Microdevices 10:251–257. https://doi.org/10.1007/s10544-007-9131-x

Kang JH, Park J-K (2007) Magnetophoretic continuous purification of single-walled carbon nanotubes from catalytic impurities in a microfluidic device. Small 3:1784–1791. https://doi.org/10.1002/smll.200700334

Karim MR, Rhodes ER, Brinkman N, Wymer L, Fout GS (2009) New electropositive filter for concentrating enteroviruses and noroviruses from large volumes of water. Appl Environ Microbiol 75:2393–2399. https://doi.org/10.1128/aem.00922-08

Lee KS, Ram RJ (2009) Plastic-PDMS bonding for high pressure hydrolytically stable active microfluidics. Lab Chip 9:1618–1624. https://doi.org/10.1039/B820924C

Lin C-C, Chen A, Lin C-H (2008) Microfluidic cell counter/sorter utilizing multiple particle tracing technique and optically switching approach. Biomed Microdevices 10:55–63. https://doi.org/10.1007/s10544-007-9109-8

Liu P, Hill VR, Hahn D, Johnson TB, Pan Y, Jothikumar N, Moe CL (2012) Hollow-fiber ultrafiltration for simultaneous recovery of viruses, bacteria and parasites from reclaimed water. J Microbiol Methods 88:155–161. https://doi.org/10.1016/j.mimet.2011.11.007

McCloskey KE, Chalmers JJ, Zborowski M (2003) Magnetic cell separation: characterization of magnetophoretic mobility. Anal Chem 75:6868–6874. https://doi.org/10.1021/ac034315j

Mull B, Hill VR (2009) Recovery and detection of *Escherichia coli* O157:H7 in surface water, using ultrafiltration and real-time PCR. Appl Environ Microbiol 75:3593–3597. https://doi.org/10.1128/aem.02750-08

Park S, Zhang Y, Wang T-H, Yang S (2011) Continuous dielectrophoretic bacterial separation and concentration from physiological media of high conductivity. Lab Chip 11:2893–2900. https://doi.org/10.1039/C1LC20307J

Puchberger-Enengl D, Podszun S, Heinz H, Hermann C, Vulto P, Urban GA (2011) Microfluidic concentration of bacteria by on-chip electrophoresis. Biomicrofluidics 5:044111. https://doi.org/10.1063/1.3664691

Rajal VB, McSwain BS, Thompson DE, Leutenegger CM, Kildare BJ, Wuertz S (2007) Validation of hollow fiber ultrafiltration and real-time PCR using bacteriophage PP7 as surrogate for the quantification of viruses from water samples. Water Res 41:1411–1422. https://doi.org/10.1016/j.watres.2006.12.034

Rutjes SA, Italiaander R, van den Berg H, Lodder WJ, Husman AMD (2005) Isolation and detection of enterovirus RNA from large-volume water samples by using the NucliSens miniMAG system and real-time nucleic acid sequence-based amplification. Appl Environ Microbiol 71:3734–3740. https://doi.org/10.1128/aem.71.7.3734-3740.2005

Satyanarayana S, Karnik RN, Majumdar A (2005) Stamp-and-stick room-temperature bonding technique for microdevices. J Microelectromech Syst 14:392–399. https://doi.org/10.1109/JMEMS.2004.839334

Su Y, Li C, Zhao W, Shi Q, Wang H, Jiang Z, Zhu S (2008) Modification of polyethersulfone ultrafiltration membranes with

phosphorylcholine copolymer can remarkably improve the anti-fouling and permeation properties. J Memb Sci 322:171–177. https://doi.org/10.1016/j.memsci.2008.05.047

Thorsen T, Maerkl SJ, Quake SR (2002) Microfluidic large-scale integration. Science 298:580–584. https://doi.org/10.1126/science.1076996

Wang S, Sarenac D, Chen MH, Huang S-H, Giguel FF, Kuritzkes DR, Demirci U (2012) Simple filter microchip for rapid separation of plasma and viruses from whole blood. Int J Nanomed 7:5019–5028. https://doi.org/10.2147/IJN.S32579

Wu D, Steckl AJ (2009) High speed nanofluidic protein accumulator. Lab Chip 9:1890–1896. https://doi.org/10.1039/B823409D

Zhang J, Mahalanabis M, Liu L, Chang J, Pollock N, Klapperich C (2013a) A disposable microfluidic virus concentration device based on evaporation and interfacial tension. Diagnostics 3:155–169

Zhang Y, Riley LK, Lin M, Purdy GA, Hu Z (2013b) Development of a virus concentration method using lanthanum-based chemical flocculation coupled with modified membrane filtration procedures. J Virol Methods 190:41–48. https://doi.org/10.1016/j.jviromet.2013.03.017

Zheng S, Lin H, Liu J-Q, Balic M, Datar R, Cote RJ, Tai Y-C (2007) Membrane microfilter device for selective capture, electrolysis and genomic analysis of human circulating tumor cells. J Chromatogr A 1162:154–161. https://doi.org/10.1016/j.chroma.2007.05.064